

No Significant Effect of Coulomb Stress on the Gutenberg-Richter Law after the Landers Earthquake

Víctor Navas-Portella,^{1,2,3} Abigail Jiménez,⁴ and Álvaro Corral^{1,2,5,6}

¹*Centre de Recerca Matemàtica, Edifici C,
Campus Bellaterra, E-08193 Barcelona, Spain*

²*Barcelona Graduate School of Mathematics, Edifici C,
Campus Bellaterra, E-08193 Barcelona, Spain*

³*Facultat de Matemàtiques i Informàtica,
Universitat de Barcelona, Barcelona, Spain*

⁴*Departamento de Computación e Inteligencia Artificial. Universidad de Granada. Campus Ceuta C/. Cortadura del Valle s.n., 51001 Ceuta, Spain*

⁵*Departament de Matemàtiques, Universitat Autònoma de Barcelona, E-08193 Barcelona, Spain*

⁶*Complexity Science Hub Vienna, Josefstädter Straße 39, 1080 Vienna, Austria*

Abstract

Coulomb-stress theory has been used for years in seismology to understand how earthquakes trigger each other. Whenever an earthquake occurs, the stress field changes, and places with positive increases are brought closer to failure. Earthquake models that relate earthquake rates and Coulomb stress after a main event, such as the rate-and-state model, assume that the magnitude distribution of earthquakes is not affected by the change in the Coulomb stress. By using different slip models, we calculate the change in Coulomb stress in the fault plane for every aftershock after the Landers event (California, USA, 1992, moment magnitude 7.3). Applying several statistical analyses to test whether the distribution of magnitudes is sensitive to the sign of the Coulomb-stress increase we conclude that no significant effect is observable. Further, whereas the events with a positive increase of the stress are characterized by a much larger proportion of strike-slip events in comparison with the seismicity previous to the mainshock, the events happening despite a decrease in Coulomb stress show no relevant differences in focal-mechanism distribution with respect to previous seismicity.

INTRODUCTION

Since the L’Aquila event in 2009 seismologists have advocated the modeling and testing of earthquakes within a rigorous statistical framework [1], following on the CSEP (Collaboratory for the Study of Earthquake Predictability) previous works. A recent pseudo-prospective forecast was conducted on the 2010-2012 Canterbury, New Zealand, series, in order to test a total of fourteen earthquake models [2, 3]. Its results offer some encouragement for a physical basis in earthquake forecasting and suggest that some of the recent physics-based and hybrid model development have added informative components [4].

Our basic understanding of earthquake physics is that stress is being accumulated on certain regions due to different mechanisms, and that those regions rupture whenever that stress surpasses the strength of the material. That rupture is the earthquake. The mechanisms by which stresses change are diverse: in addition to tectonic driving, they can be induced by precedent earthquakes [5–9], by volcanic activity [10], or even by artificial means, such as injection of fluids [11] or aquifer withdrawal [12]. Coulomb-stress theory has been used to forecast spatial patterns of aftershock rates, as well as assessing the likelihood of earthquake rupture sequences [13, 14]. Although there exist instances where its predictive skills are arguable [15–18], the monitoring of the changes in the stress field represents a valuable information for seismic and volcanic hazard forecasting and to proposing the adequate mitigation measures.

A hallmark of statistical seismology and of earthquake hazard assessment is the well-known Gutenberg-Richter relation, or Gutenberg-Richter law [19–21]. This law states that earthquake magnitudes must be described in terms of a probability distribution and that, above a lower cut-off value, this distribution is exponential. In terms of the probability density $f(m)$ one has

$$f(m) = (b \ln 10) 10^{-b(m-m_{min})} \propto 10^{-bm},$$

defined for $m \geq m_{min}$ (values below m_{min} are disregarded), with m the magnitude, m_{min} the lower cut-off in magnitude, b the so called b -value (directly related to the exponent β of the power-law cumulative distribution of seismic moment, $\beta = 2b/3$), and the symbol \propto denoting proportionality. (This relation is usually called magnitude-frequency distribution in seismology). A straightforward property of the exponential distribution leads to the fact that the rate (the number per unit time of earthquakes above a certain magnitude m) is

also a decreasing exponential function of the magnitude, with the same b -value.

Earthquake hazard forecasts usually comprise two stages: in the first one, the rate of events is forecasted, while in the second one, the Gutenberg-Richter law is applied to those rates in order to obtain the probabilities of occurrence for each magnitude threshold. In the case of physics-based models, the forecasted rates of events depend on the Coulomb stresses calculated in the region of interest. These models are variants of the rate-and-state model by Dieterich [22],

$$R(t) = r [1 + (e^{-\Delta CFS/B} - 1) e^{-t/t_a}]^{-1} \quad (1)$$

where $R(t)$ is the rate of events (i.e., aftershocks) at any given time t after a mainshock, r is the rate of background seismicity, ΔCFS is the increase in Coulomb stress induced by the mainshock, B is a constant, for our purposes, and t_a is the characteristic relaxation time [22].

Note that in the application of the Gutenberg-Richter law to the forecasted rate $R(t)$ given by the previous expression it is implicit that the Coulomb-stress change caused by a mainshock does not alter the fulfillment of the Gutenberg-Richter law for the aftershocks, in particular, this law remains the same no matter whether ΔCFS is positive or negative. In some sense, $R(t)$ inherits the dependence of the background rate r with the magnitude. Therefore, the rate-and-state formulation [14, 22–26] assumes the fulfillment of the Gutenberg-Richter law for the incoming events (aftershocks), with no change in the b -value. This assumption is made when inverting earthquake rates to obtain stress changes [10, 27, 28]. Physics-based models also assume the magnitude distribution does not depend on the stress values, so that forecasted rates can be translated into probabilities of occurrence for different magnitudes.

In fact, it has been long debated [29] whether the value of b in the Gutenberg-Richter law is essentially universal [21] or whether, on the contrary, it is affected by different geophysical conditions. Some studies [30, 31] have correlated the b -value (and also the parameters of the Omori law [32–34]) with the style of faulting [35]. These studies indicate that (at least for California, for a long time period) $b \approx 1.03$ for normal events, $b \approx 0.87$ for strike-slip events, and $b \approx 0.79$ for thrust events [30]. As the b -value is directly related to the log-ratio between the number of small and large earthquakes, variations in b can be associated with the ability of an earthquake rupture to propagate (more large events, low b) or not (less large events, high b).

According to Mohr-Coulomb theory [31, 36], thrust faults rupture at much higher stress than normal faults (with strike-slip faults in between, assuming the same value for the coefficient of static friction). When the stress required to initiate a rupture is higher, stress interactions are enhanced and cracks can propagate faster in many different directions, yielding larger earthquakes [31], consistent with the empirically observed b -values for thrust faulting [30]. Conversely, for lower rupture thresholds, one should find indeed the large b -values characterizing normal faulting. Although the threshold for triggering might be different for the different styles of faulting, the rupture or not of a fault also depends on its previous state.

Here we investigate, with rigorous statistical tools, if the Gutenberg-Richter law is affected by the binary choice between positive and negative increases of the Coulomb stress, using the sequence of events after the 1992 Landers earthquake. The next section explains the seismic catalog and the spatio-temporal window used to define this sequence. Section 3 develops the procedure to calculate the increase in the Coulomb stress that the Landers earthquake provokes in the fault plane of each event in the sequence. The statistical analysis is also exposed in this section. Section 4 presents the results and Sec. 5 summarizes the conclusions.

DATA

The June 28, 1992, Landers earthquake, with a moment magnitude $m = M_w = 7.3$ and a rake angle $\rho = -177^\circ$, corresponding to strike-slip focal mechanism, has been the strongest one in Southern California at least since 1952. The earthquake and its subsequent aftershock sequence have been extensively studied [37–39], with a number of slip distributions that describe its rupture [40–43]. In this work we use four slip models to calculate the strain; these models are: Wald and Heaton (referred here to as **wald**) [40], Hernandez et al. (**hernandez**) [41], Landers Big-Bear California (**lbbcal**) [42] and Landers Surface Rupture (**lsurfrup**) [43]. The terminology is the same as the one used in Ref. [42].

High quality catalogs for Southern California are nowadays available [44, 45]; in particular in this paper we will select the Landers’ aftershocks from the Yang-Hauksson-Shearer (YHS) catalog [46], which incorporates focal-mechanism solutions. Given the distribution of acceptable mechanisms, the preferred solution is the most probable one [47]. The ambiguity of the actual fault plane is solved by considering that the preferred nodal planes are those

associated with the preferred solution listed in the catalog [46]. The focal mechanism, in concrete, the rake angle, together with Landers stress field derived from the slip model, allows us to calculate Coulomb-stress increases (positive or negative) induced by the mainshock on the actual orientations of the aftershock ruptures. Note that the YHS catalog does not report the moment magnitude necessarily but a preferred magnitude.

In order to better detect the influence of the Landers stress change we take a time window of 100 days after the mainshock and a spatial window going from 10 to 150 km from the Landers rupture. Landers earthquake is taken as the mainshock for all the slip models except for the lbbcal whose mainshock is the Big-Bear earthquake (which occurred approximately three hours after Landers earthquake with a moment magnitude $m = M_w = 6.3$ and rake angle $\rho = -180^\circ$ [42]). We tried other choices for the limits of the window finding similar results as reported in the Supplementary Material. This spatio-temporal window defines Landers aftershocks for our purposes. Distances to the fault are computed as the minimum Euclidean distance from the aftershock hypocenter to the center of each fault patch as given by the slip model. The reason to exclude events closer than 10 km is the uncertainty of the deformation field near the edges of the subfaults [48], as the finite-fault approximation provides spurious values near the fault zone because of boundary effects.

PROCEDURE

The dMODELS software in Ref. [49] calculates the deformation field (or displacement) caused by different models corresponding to different physical processes. Although there exist many programs that calculate deformation caused by earthquakes, this package has been thoroughly tested, and can introduce many different sources of deformation, which can be translated into stress changes in a straightforward way. The dMODELS software will be the one used here to obtain deformation field from the different slip models of Landers.

The local coordinate system for dMODELS is east-north-up, ENU. After introducing the corresponding slip model (also called source model) for the mainshock of interest (Landers in our case [42]) into the dMODELS program we obtain the projections in the ENU axes of the deformation field \vec{u} caused by the mainshock at the position of each aftershock (and also at its neighborhood, in order to take spatial derivatives). We then obtain the strain tensor associated to \vec{u} by calculating the (symmetrized) gradient of the deformation [50],

whose components are $\varepsilon_{ij} = (\nabla_i u_j + \nabla_j u_i)/2$ (with a spatial step equal to 1 km).

Afterwards, we assume an isotropic and elastic material for calculating the stress tensor [50], or, more precisely, the contribution of the mainshock to the stress tensor, $s_{ij} = 2\mu\varepsilon_{ij} + \lambda\delta_{ij}\sum_k \varepsilon_{kk}$, with δ_{ij} the components of the identity matrix and with the Lamé elastic moduli given by $\mu = \lambda = 3 \times 10^4$ MPa [36] (Poisson ratio $\nu = \lambda(\lambda + \mu)^{-1}/2 = 0.25$). Moreover, when calculating the stress induced by previous events (mainshocks) on new events (aftershocks) it is necessary to orientate it onto the fault [51, 52], so that one can actually evaluate if the new events could have been triggered by the induced stress or not. Given the fault plane and slip vector of an aftershock, we calculate the change in the normal σ_n and shear (or tangential) τ stresses in that orientation and position, as

$$\Delta\sigma_n = \sum_{ij} n_i s_{ij} n_j \text{ and } \Delta\tau = \sum_{ij} \ell_i s_{ij} n_j, \quad (2)$$

with n_i and ℓ_i the components of the normal and slip vectors, respectively. The formulas to obtain the ENU components of these vectors from the information recorded in the YHS catalog (strike, dip and rake angles [53]) are given in the Methods section. Note that in order to be realistic, the Coulomb-stress changes have to be calculated onto the planes of the actual faults [51]. This contrasts with an approach in which Coulomb stresses are calculated onto the so-called optimally oriented planes [6], when the only information available is the regional stress. However, optimally oriented planes are imaginary planes that might not correspond to the actual geology.

The Mohr-Coulomb failure criterion [54] states that the shear stress τ on a fault that ruptures must surpass the critical value τ_c , which is a linear function of the normal stress,

$$\tau_c = C - \mu'\sigma_n \quad (3)$$

with C the cohesion and μ' the effective fault friction coefficient (including the contribution of the pore pressure [6, 55]). Care must be taken with the convention of signs in the normal stress, which is not the same in geophysics than in solid mechanics (our convention takes the negative sign for compression, this is the reason for the negative sign before μ'). From this failure criterion it is natural to define the Coulomb stress as $CFS = \tau + \mu'\sigma_n$, which signals failure by $CFS > C$. In fact, for pre-existing faults one can consider that the cohesion is nearly zero. The change in Coulomb stress at the aftershock fault plane due to the mainshock will be

$$\Delta CFS = \Delta\tau + \mu'\Delta\sigma_n, \quad (4)$$

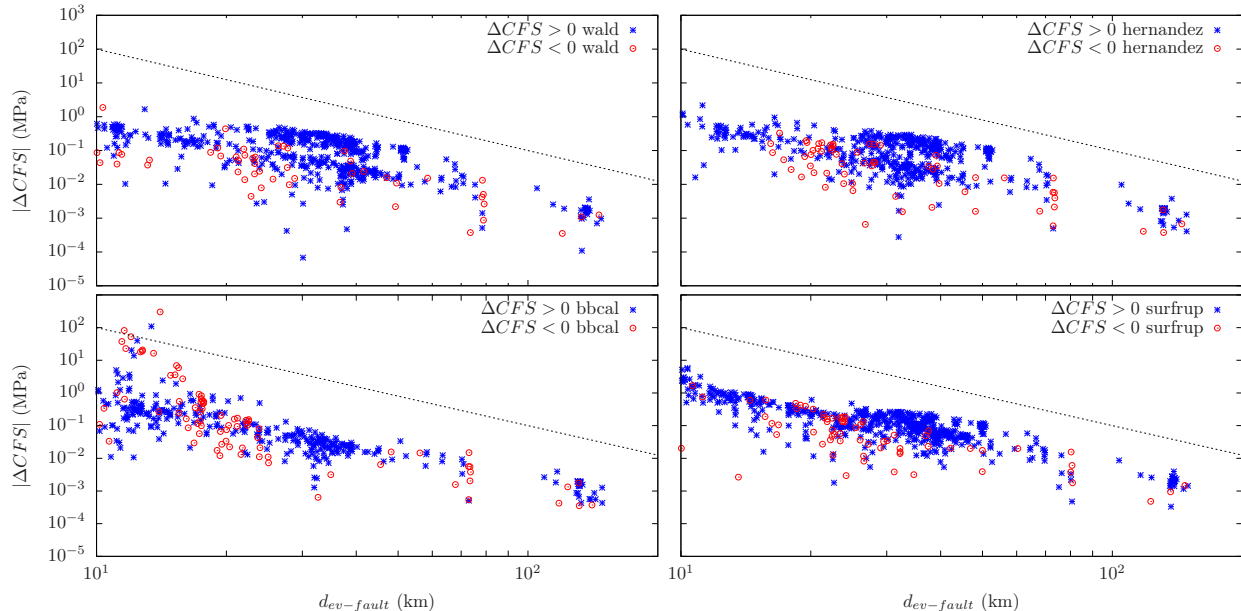


FIG. 1. Dependence of the absolute value of the change in the Coulomb stress ΔCFS as a function of the distance to the fault of the aftershocks for each slip model, $m_{min} = 3$ and $\mu' = 0.4$. Aftershocks correspond to the first 100 days after the Landers mainshock. Distance of aftershocks to the Landers rupture is restricted to be between 10 and 150 km. Black dashed line with slope -3 , as stated by Coulomb theory, is shown as a guide to the eye.

with $\Delta\tau$ and $\Delta\sigma_n$ coming from Eq. (2). Thus, positive increases of the Coulomb stress bring the fault closer to failure, whereas negative increases distance it away from failure. As the real value of the effective friction coefficient μ' is uncertain [36], we will check different values of it as in Ref. [15]. In Fig.1 we present a scatter plot that illustrates the dependence of the absolute value of the increase of Coulomb stress $|\Delta CFS|$ as a function of the distance to the fault $d_{ev-fault}$ for the four slip models. As it is implicit by the Coulomb theory, the value of the increase of Coulomb stress decays as the cube of the distance to the fault. In Fig.2 we show aftershocks with positive and negative increase of Coulomb stress placed in the window we study for the wald slip model and $\mu' = 0.4$.

Once we know the Coulomb-stress change in the fault plane of each aftershock we can separate these into two subsets attending to the value of the change, with the most natural separation being between positive and negative increases (denoted by sub-indexes $>$ and $<$, respectively). Naturally, we expect to obtain many more aftershocks in positive lobes than in negative ones [56]. It is for each of these subsets that we will study the fulfilment of

the Gutenberg-Richter law. For any set or subset (or sub-catalog) of earthquakes, the value of b in the Gutenberg-Richter law can be automatically obtained by maximum-likelihood estimation, as [57, 58]:

$$b = \frac{\log_{10} e}{\bar{m} - m_{min}}, \quad (5)$$

with \bar{m} the mean magnitude of the events considered (i.e., those above m_{min}). Let us stress that m_{min} is not the minimum magnitude recorded in the catalog but the value from which we fit the Gutenberg-Richter law to the data. As the resolution of the magnitude Δm is small ($\Delta m = 0.01$) it is not necessary to perform the discreteness correction [59].

In principle, results should not significantly depend on the value of m_{min} , but the larger its value the less data to calculate the b -value and the larger the uncertainty, whereas for a too small m_{min} the Gutenberg-Richter law would not be fulfilled due to the incompleteness of the catalog and the resulting b -value would be artefactual. In this paper we have taken $m_{min} = 3$, which ensures the fulfilment of the Gutenberg-Richter law for all data sets analysed, as we have verified by means of the Kolmogorov-Smirnov goodness-of-fit test [60], where the distribution of the test statistic and, from it, the p -value of the fit, p_{fit} , is calculated using 10^4 Monte Carlo simulations [61, 62]. Although some fitting procedures look for the value of m_{min} that optimizes the fit for a given data set [61–63], we have opted for a fixed m_{min} in order to compare the different subsets on the same footing. So, in all cases the exponential fit for $m \geq 3$ cannot be rejected (p -value of the test larger than 0.05). Note that m_{min} defined in this way can be considered a magnitude of completeness, and thus, our value of m_{min} turns out to be rather conservative or strict, in the sense that it is larger (and therefore safer) than in other works [64].

The maximum-likelihood estimation of the b -value has an associated uncertainty given by its standard deviation

$$\sigma = \frac{b}{\sqrt{N}},$$

where N is the number of earthquakes with $m \geq m_{min}$ in the subset, out of a total number N_{tot} (of any magnitude) [65]. Note that this uncertainty only depends on the number of data, and has nothing to do with the goodness of the fit. This result, as well as the formula for the maximum-likelihood estimation of b , Eq. (5), can also be obtained from Ref. [62] just taking into account the relation between moment magnitude and seismic moment. This standard deviation, σ , is what represents the uncertainty when we report our resulting b -values.

The comparison between the b -values of the subsets with different values of ΔCFS is done by means of the following statistic

$$z = \frac{b_{>} - b_{<}}{\sqrt{\sigma_{>}^2 + \sigma_{<}^2}} = \frac{b_{>} - b_{<}}{\sqrt{b_{>}^2/N_{>} + b_{<}^2/N_{<}}},$$

where the sub-indexes $>$ and $<$ refer to positive and negative increases of the Coulomb stress. This statistics is rooted on the null hypothesis that both subsets of data (positive and negative) belong to the same underlying population of earthquake magnitudes and then, both estimators of the b -value ($b_{>}$ and $b_{<}$) have a common mean value, which is that of the whole population. Therefore, under the null hypothesis, $b_{>} - b_{<}$ has zero mean and standard deviation $\sqrt{\sigma_{>}^2 + \sigma_{<}^2}$ (approximating the population variance from the sample values of $b_{>}$ and $b_{<}$ and assuming zero covariance between $b_{>}$ and $b_{<}$) and then z has zero mean too and unit standard deviation. An additional assumption is that z is normally distributed, which is supported by theory in the asymptotic limit ($N_{>}$ and $N_{<}$ going to infinity [66]). Assuming normality we will test the null hypothesis just comparing the value of z with the standard normal distribution and the hypothesis will be rejected if the value of z is too extreme for a given significance level; in quantitative terms this will be given by a p -value, called p_{norm} , smaller than the significance level (0.05, let us say; corresponding to 0.95 confidence).

If we do not want to believe that the asymptotic regime has been reached the best option is to use a permutation test [67]. Under the null hypothesis (all values of magnitude belong to the same population) one is allowed to aggregate both subsets (positive and negative) and take, without repetition, two sub-samples of size $N_{>}$ and $N_{<}$; note that this is equivalent to take a permutation of the aggregated sample and separate it into two parts ($>$ and $<$). One proceeds in the same way as in the original data, calculating (by maximum likelihood) $b_{>}^*$, $b_{<}^*$, and from here $\sigma_{>}^*$, $\sigma_{<}^*$, and z^* , where the asterisk marks that we are dealing with a permutation of the original data. Repeating the permutation procedure many times we find the distribution of z^* , which can be compared with the original value z . The p -value of the permutation test, p_{perm} , will be given by the fraction of permutations for which $|z^*|$ is larger than $|z|$ (the empirical value). In our case we take 10^4 permutations.

As a complement, instead of the fitted b -values we may directly compare the distributions; this can be done with the two-sample Kolmogorov-Smirnov test, whose null hypothesis is that both data sets come from the same population, so, the two empirical distributions ($>$ and $<$) are two realizations of a unique theoretical distribution (which remains unveiled)

[60]. This test leads to a p -value that we call p_{2ks} . A final comparison comes from the application of the Akaike information criterion (AIC) [68]. We consider that we aggregate both subsets (positive and negative ΔCFS) but keeping the distinction in the sign of ΔCFS . Then, we contemplate two options. Model 1, simple: we fit the aggregated data set with one single Gutenberg-Richter exponential leading to the value b_{all} . Model 2, “complex”: we fit each data set with its own exponential function (values $b_>$ and $b_<$ in the same table). In each case, $AIC = 2k - 2\hat{\ell}$, where k is the number of parameters of each model and $\hat{\ell}$ is the log-likelihood of the model at maximum. The likelihood in model 2 is the sum of likelihoods for each subcatalog [66]. The model yielding the smallest AIC should be preferred. Defining $\Delta AIC = AIC_2 - AIC_1$ leads to the rejection of the simple model when ΔAIC is significantly below zero (see next section).

RESULTS

Table I shows the values of b obtained from the application of the maximum likelihood estimation and goodness-of-fit test explained above to the different subcatalogs obtained from the Landers sequence. We can see how, in the overall case (when events are not separated in terms of Coulomb-stress change), the Gutenberg-Richter law is fulfilled with an average value $b_{all} = 0.92$. Each slip model leads to a different value of b_{all} because the fault geometry is different, and events too close to the fault are discarded. This b -value for the Landers aftershocks is found, not surprisingly, to be close to the average for aftershocks in California, $b \simeq 0.9$ [69, 70], and somewhat below the long-term value of Southern California (all events), $b \simeq 1.0$ [71] (although other works report $b \simeq 1.0$ for Landers aftershocks, probably due to the consideration there of a much smaller magnitude of completeness [72]).

After separating by the sign of the Coulomb-stress change, the first result that becomes apparent from the table is that the number of aftershocks with positive increases is much larger than the number for the negative case [6, 7], no matter neither the slip model (nor the value of μ') used to calculate ΔCFS . Regarding the b -values, although they depend on the slip model, we can summarize them by taking the mean of the four models and taking $\mu' = 0.4$ as $b_> \simeq 0.93$ and $b_< \simeq 0.87$ with individual uncertainties around 0.04 and 0.11 respectively. Note that the magnitude distribution for the overall case is a mixture of the distributions corresponding to $\Delta CFS > 0$ and $\Delta CFS < 0$, and therefore, the value of b in

the overall case turns out to be the harmonic mean of $b_{>}$ and $b_{<}$, i.e.,

$$b_{all}^{-1} = \frac{N_{>}b_{>}^{-1} + N_{<}b_{<}^{-1}}{N_{>} + N_{<}}, \quad (6)$$

see Refs. [73?]. Despite the fact the values of $b_{>}$ and $b_{<}$ do not look much different between them, statistical testing becomes necessary in order to establish significance [74].

Table II compares $b_{>}$ and $b_{<}$ for the different slip models taking $\mu' = 0.4$, and shows that the difference in the b -values can not be considered significantly different from zero with a confidence larger than 0.95 so, the null hypothesis $b_{>} \simeq b_{<}$ can not be rejected. This result is true for all the statistical tests as all the p -values are greater than 0.05. Table II also shows the results of the two-sample Kolmogorov-Smirnov test and the calculation of ΔAIC leading in both cases to the result that no change in the distributions as a function of positive and negative ΔCFS can be established. In concrete, ΔAIC is always greater than the critical value $\Delta AIC_c = -1.84$ [68, 75] at significance level of 0.05. The wald slip model is the one for which both distributions (positive and negative) appear as more different; however, the difference is not significant. Figure 3 shows the probability density functions as well as the complementary cumulative probability functions in this case.

As mentioned in the introduction, some authors have unveiled a direct dependence of the b -value on the focal mechanism of the events, which implies a dependence of b on the total stress (not the stress increase) [30]. The rake angle is associated to the focal mechanism in the following way: values of the rake around -90° correspond to normal events (labelled as *no*), values around 0° or $\pm 180^\circ$ to strike-slip events (*ss*), and values around 90° to thrust events (*th*). We do not find any significant effect of the rake on the b -value (See Table III), due to the low number of events in the normal and thrust regimes (which increases the uncertainty). But despite the large uncertainty, the values of b_{no} and b_{ss} are roughly in agreement with the results of Ref. [30]; however, our value of b_{th} turns out to be rather large in comparison (but compatible, within the error bars). We further observe that ratios $N_{>ss}/N_{<ss}$ and $N_{>no}/N_{<no}$ are higher than $N_{>th}/N_{<th}$; i.e., in strike-slip and normal events the contribution from $\Delta CFS > 0$ is higher than in thrust events, as can be verified looking at Table III. Comparing with the number of earthquakes with each focal mechanism for the 5 years previous to Landers we conclude that it is indeed the low number of thrust aftershocks with positive ΔCFS which is anomalous (and not the relatively high number of them for negative ΔCFS), due to an increase in the number of normal events and an even

higher increase in strike-slip events triggered ($\Delta CFS > 0$) by the Landers mainshock. This difference in numbers becomes visually apparent in Fig. 2.

Slip Model		N_{tot}	N	b -value	σ	p_{fit}
wald	$\Delta CFS > 0$	5213	509	$b_{>} = 0.927$	0.041	0.313 ± 0.005
	$\Delta CFS < 0$	814	51	$b_{<} = 0.766$	0.107	0.861 ± 0.003
	All	6027	560	$b_{all} = 0.909$	0.038	0.243 ± 0.004
hernandez	$\Delta CFS > 0$	5027	465	$b_{>} = 0.926$	0.043	0.505 ± 0.005
	$\Delta CFS < 0$	765	62	$b_{<} = 0.866$	0.110	0.197 ± 0.004
	All	5792	527	$b_{all} = 0.919$	0.040	0.231 ± 0.004
bbcal	$\Delta CFS > 0$	3641	309	$b_{>} = 0.978$	0.056	0.232 ± 0.004
	$\Delta CFS < 0$	1191	82	$b_{<} = 0.948$	0.105	0.327 ± 0.005
	All	4832	391	$b_{all} = 0.971$	0.049	0.053 ± 0.002
surfrup	$\Delta CFS > 0$	5534	548	$b_{>} = 0.890$	0.038	0.290 ± 0.005
	$\Delta CFS < 0$	774	68	$b_{<} = 0.891$	0.108	0.555 ± 0.005
	All	6308	616	$b_{all} = 0.890$	0.036	0.239 ± 0.004

TABLE I. Results of fitting the Gutenberg-Richter law to the Landers aftershocks, separating positive and negative Coulomb-stress increases, for different Slip models, $\mu' = 0.4$ and $m_{min} = 3$. Aftershocks correspond to the first 100 days after the Landers mainshock. Distance of aftershocks to the Landers rupture is restricted to be between 10 and 150 km. The p -value of the goodness-of-fit test is computed with 10^4 simulations and is denoted by p_{fit} . Its uncertainty corresponds to one standard deviation. In no case the Gutenberg-Richter law can be rejected.

DISCUSSION

We have seen how the positive Coulomb-stress increase associated to the Landers mainshock triggered a very large number of strike-slip events and also a large number of normal events, but much less thrust events. Although this result seems easy to establish, as it can be obtained without the calculation of ΔCFS (due to the fact that most of the events have $\Delta CFS > 0$ and thus, this subset dominates the overall statistics), we have unambiguously associated these events to the positive ΔCFS . On the other side, the events in the opposite

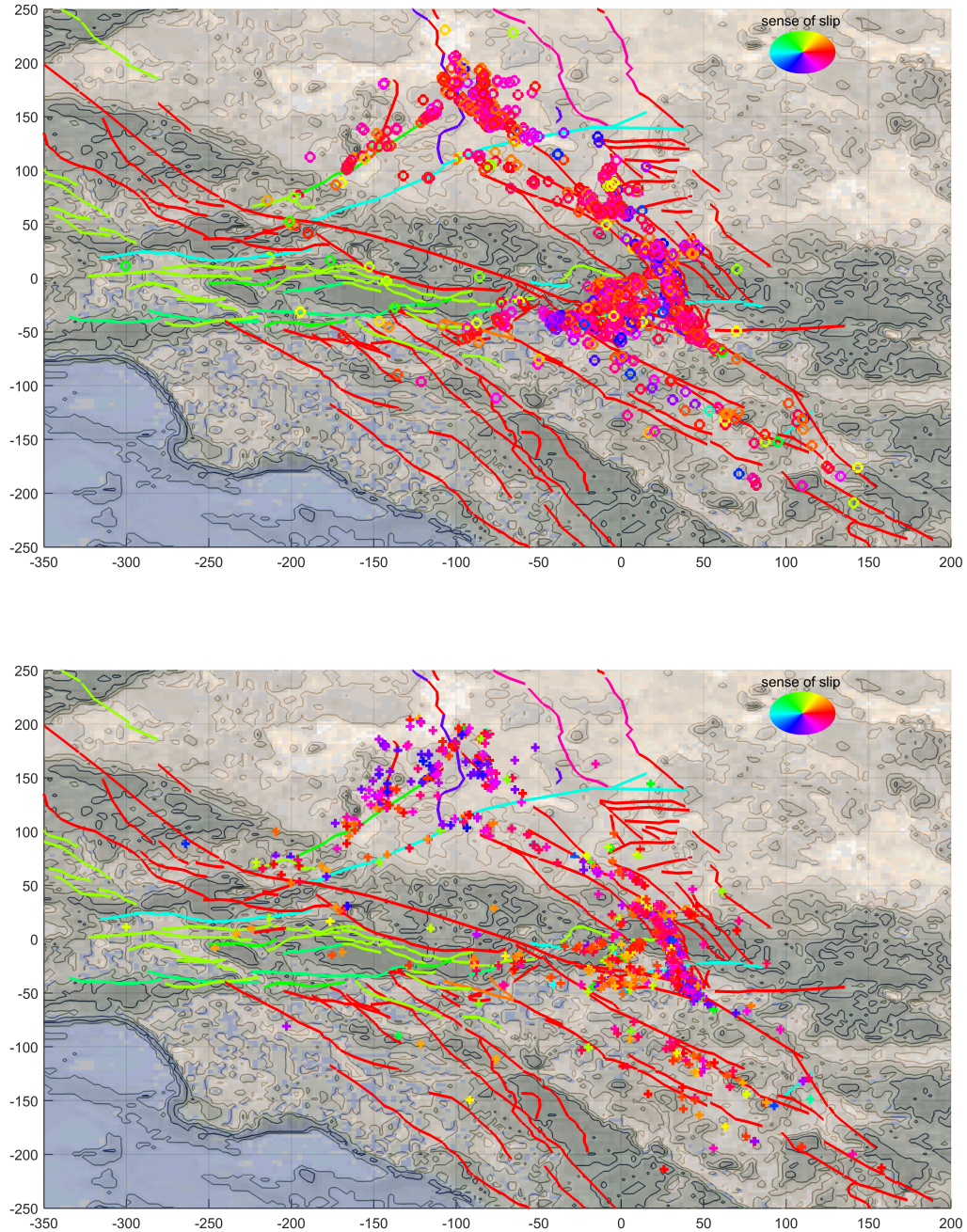


FIG. 2. Rakes of Landers aftershocks compared to the fault network (time window of 100 days after the mainshock). Top: $\Delta CFS > 0$. Bottom: $\Delta CFS < 0$. Color scale for the sense of slip: red for right-lateral (ρ close to $\pm 180^\circ$), light blue for left-lateral (ρ close to 0°), green for normal (ρ close to -90°) and dark blue or purple for thrust faulting (ρ close to 90°). No restriction on the magnitude values is used. An area of 550×500 km is shown.

Slip Model	z	p_{norm}	p_{perm}	d_{2ks}	p_{2ks}	ΔAIC
wald	1.396	0.163	0.156 ± 0.004	0.139	0.311	0.234
hernandez	0.511	0.609	0.596 ± 0.005	0.095	0.690	1.748
bbcal	0.254	0.800	0.828 ± 0.004	0.063	0.952	1.936
surfrup	-0.010	0.992	0.994 ± 0.001	0.094	0.643	1.999

TABLE II. Results of the statistical tests comparing b -values and magnitude distributions for positive and negative Coulomb-stress changes, using different slip models and $\mu' = 0.4$. Values of $\Delta AIC = AIC_2 - AIC_1$ are also included. Same data as previous table. Columns 2 to 4: testing the null hypothesis that there is no difference between the b -values (i.e., $b_> = b_<$). Columns 5 to 6: testing the null hypothesis that there is no difference in the distributions, using the 2-sample Kolmogorov-Smirnov test. In the first test, both asymptotic normality of the z statistic and a permutation test are used for the calculation of the p -value (labeled as p_{norm} and p_{perm} , respectively). In the latter case the number of permutations is 10^4 , and the uncertainty of p_{perm} corresponds to one standard deviation. d_{2ks} and p_{2ks} are the Kolmogorov-Smirnov statistic and its p -value.

regime (with $\Delta CFS < 0$) keep a proportion between normal, strike-slip, and thrust events rather different to the $\Delta CFS > 0$ case, and close to that of the immediately previous record (1987-1992, up to Landers). These results are largely independent on the slip model used to calculate the change in Coulomb stress. We have also found that the b -values of the Gutenberg-Richter law for events with positive ΔCFS (for which $b_> \simeq 0.93$) are in general larger than the b -values for the events with negative ΔCFS ($b_< \simeq 0.87$); nevertheless, this difference is not statistically significant for any of the slip models used to compute the change in the Coulomb stress.

A number of extensions and improvements could be incorporated to our approach in future research. Moreover, we need to take into account the relation between b -values and differential stress [76]. We make use of slip models with relatively low resolution in space; so, it would be interesting to know if higher resolution slip models [78, 79] lead to somewhat different values of the strain and the stress, in particular close to the fault. Also, some authors have argued that real faults should have rather low values of the μ' coefficient [80]. We provide some check of this in the supplementary material, which leads to the conclusion

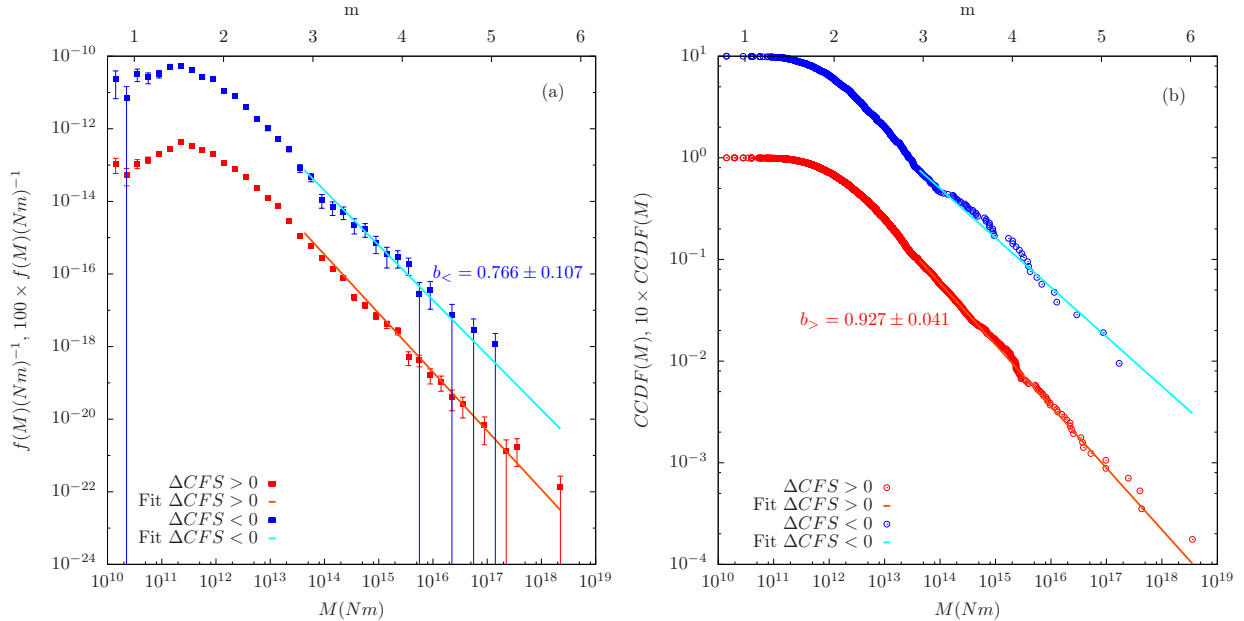


FIG. 3. Estimation of the probability densities (a) and of the complementary cumulative distribution functions (CCDF) (b) of seismic moment M for Landers aftershocks with $\Delta CFS > 0$ and $\Delta CFS < 0$ for the wald slip model using $\mu' = 0.4$ in the calculation of ΔCFS . Curves corresponding to $\Delta CFS < 0$ have been conveniently multiplied by a factor 100 and 10 respectively for clarity sake. Error bars in (a) denote one standard deviation, and are symmetric, despite the appearance in log scale, see Ref. [62].

that μ' has little influence on the b -values. Further, in our temporal window of 100 days, the effect of viscoelastic relaxation [81] should be important; so, this would need to be incorporated into the calculation of the stress. Finally, in a preliminary analysis we have seen that there is no substantial difference in the fulfilling of the Omori law [32–34] in the two populations of events ($\Delta CFS > 0$ and < 0). Indeed, if we compare this for the two subsets we find the “characteristic” power-law Omori decay of the rate with very similar values of the Omori exponent. Note that this is in disagreement with the rate-and-state formulation [22], which does not predict Omori behavior in the case of negative ΔCFS . Certainly, more research using other mainshocks (for which detailed slip models were available) is necessary, in order to reduce the statistical uncertainty by means of aggregated distributions, which could lead to the detection of small significant differences in both populations of events.

fm	$N_{>fm}$	$N_{<fm}$	N_{fm}	N_{fm}^{pre}	$b_{>fm}$	$b_{<fm}$	b_{fm}	b_{fm}^{pre}
wald								
No: $-135^\circ \leq \rho \leq -45^\circ$	39	5	$N_{no} = 44$	$N_{no}^{pre} = 77$	1.047	-	$b_{no} = 1.081$	$b_{no}^{pre} = 1.484$
Th: $45^\circ \leq \rho \leq 135^\circ$	9	8	$N_{th} = 17$	$N_{th}^{pre} = 77$	-	-	$b_{th} = 0.929$	$b_{th}^{pre} = 0.899$
SS: the rest	461	38	$N_{ss} = 499$	$N_{ss}^{pre} = 503$	0.914	0.726	$b_{ss} = 0.896$	$b_{ss}^{pre} = 0.960$
hernandez								
No: $-135^\circ \leq \rho \leq -45^\circ$	38	3	$N_{no} = 41$	$N_{no}^{pre} = 78$	0.995	-	$b_{no} = 1.011$	$b_{no}^{pre} = 1.502$
Th: $45^\circ \leq \rho \leq 135^\circ$	7	10	$N_{th} = 17$	$N_{th}^{pre} = 61$	-	-	$b_{th} = 0.929$	$b_{th}^{pre} = 0.899$
SS: the rest	420	49	$N_{ss} = 469$	$N_{ss}^{pre} = 506$	0.920	0.840	$b_{ss} = 0.911$	$b_{ss}^{pre} = 0.957$
bbcal								
No: $-135^\circ \leq \rho \leq -45^\circ$	22	4	$N_{no} = 26$	$N_{no}^{pre} = 80$	1.128	-	$b_{no} = 1.165$	$b_{no}^{pre} = 1.521$
Th: $45^\circ \leq \rho \leq 135^\circ$	7	5	$N_{th} = 12$	$N_{th}^{pre} = 69$	-	-	$b_{th} = 1.309$	$b_{th}^{pre} = 0.831$
SS: the rest	280	73	$N_{ss} = 353$	$N_{ss}^{pre} = 507$	0.970	0.886	$b_{ss} = 0.951$	$b_{ss}^{pre} = 0.958$
surfrup								
No: $-135^\circ \leq \rho \leq -45^\circ$	46	5	$N_{no} = 51$	$N_{no}^{pre} = 76$	0.939	-	$b_{no} = 0.966$	$b_{no}^{pre} = 1.470$
Th: $45^\circ \leq \rho \leq 135^\circ$	9	11	$N_{th} = 20$	$N_{th}^{pre} = 61$	-	1.010	$b_{th} = 0.886$	$b_{th}^{pre} = 0.899$
SS: the rest	493	52	$N_{ss} = 545$	$N_{ss}^{pre} = 504$	0.888	0.844	$b_{ss} = 0.884$	$b_{ss}^{pre} = 0.961$

TABLE III. Number of events and b -values corresponding to Landers aftershocks with $m \geq 3$ separated by sign of the Coulomb-stress increase ($>$ and $<$) and by focal mechanism (fm) for each slip model. $fm = no$ (normal), ss (strike-slip), and th (thrust). The Coulomb stress is calculated with $\mu' = 0.4$. Same data as in previous tables. Values of b calculated with 10 or less events are not reported. Values for the 5 years previous to Landers are also included.

METHODS

The YHS catalog characterizes fault planes and slip vectors by means of three angles: strike Θ , dip δ , and rake ρ . In term of these, the normal vector of the fault is given by

$$\hat{n} = \begin{pmatrix} n_E \\ n_N \\ n_U \end{pmatrix} = \begin{pmatrix} \cos \Theta \sin \delta \\ -\sin \Theta \sin \delta \\ \cos \delta \end{pmatrix} \quad (7)$$

in the ENU coordinate system [77]. In the same way, the slip vector is obtained as

$$\hat{\ell} = \begin{pmatrix} \ell_E \\ \ell_N \\ \ell_U \end{pmatrix} = \begin{pmatrix} \sin \Theta \cos \rho - \cos \Theta \cos \delta \sin \rho \\ \cos \Theta \cos \rho + \sin \Theta \cos \delta \sin \rho \\ \sin \delta \sin \rho \end{pmatrix}. \quad (8)$$

Note that \hat{n} and $\hat{\ell}$ are unit vectors.

SUPPLEMENTARY MATERIAL

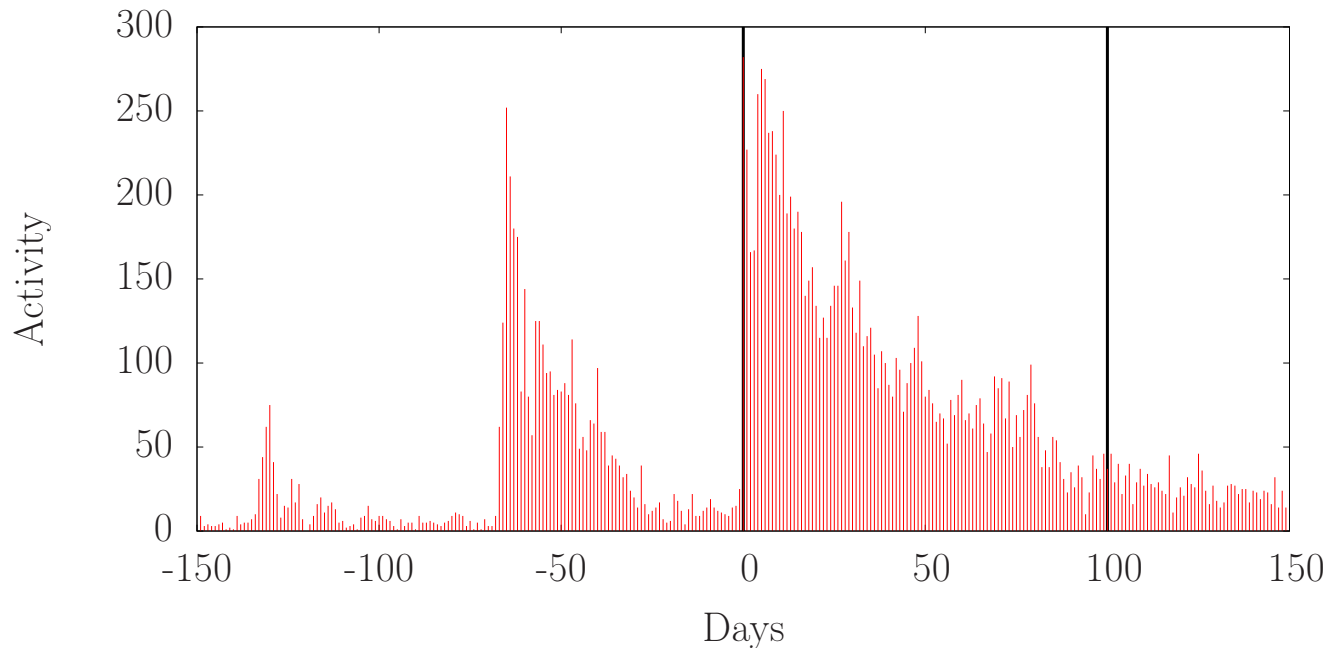


FIG. 4. Number of earthquakes per day of any magnitude before and after the Landers mainshock in the YHS catalog in the area selected for our study. Black lines show the temporal window chosen in this work.

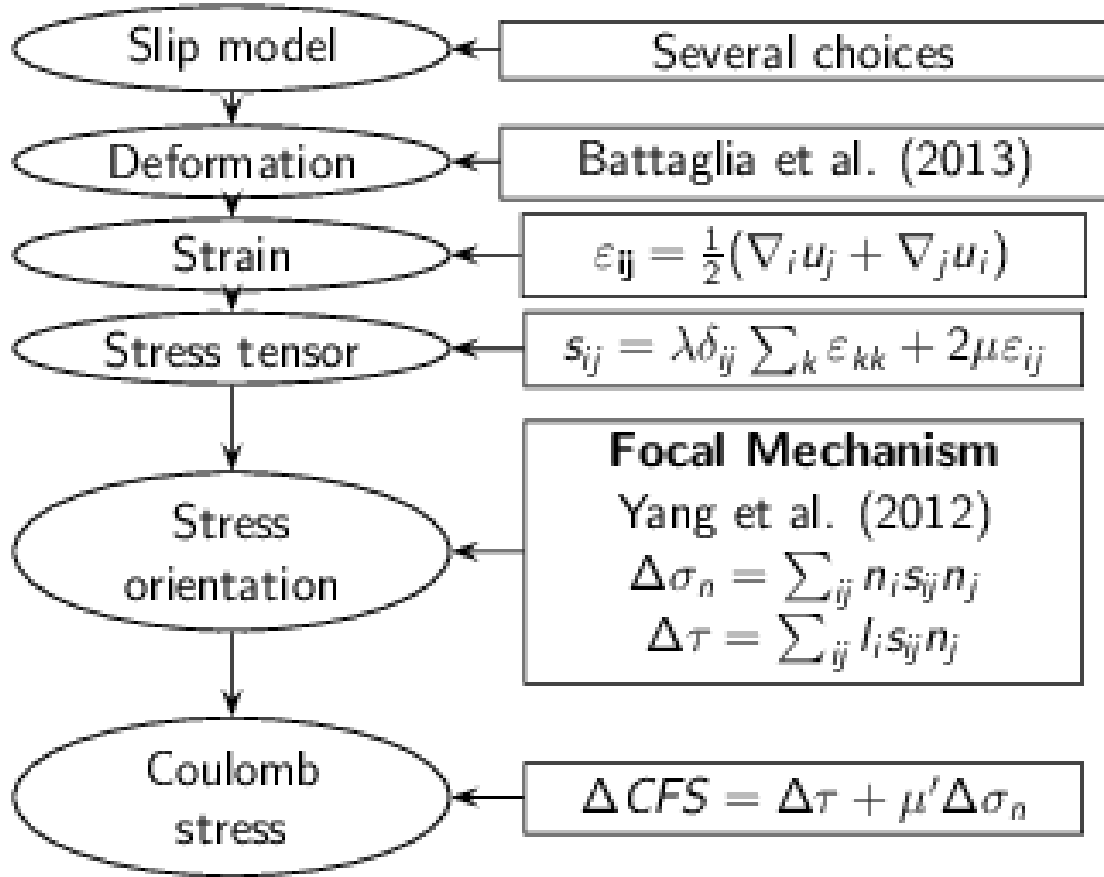


FIG. 5. Flowchart summarizing the procedure to obtain the Coulomb stress on each aftershock fault plane from the slip model and the focal-mechanism catalog.

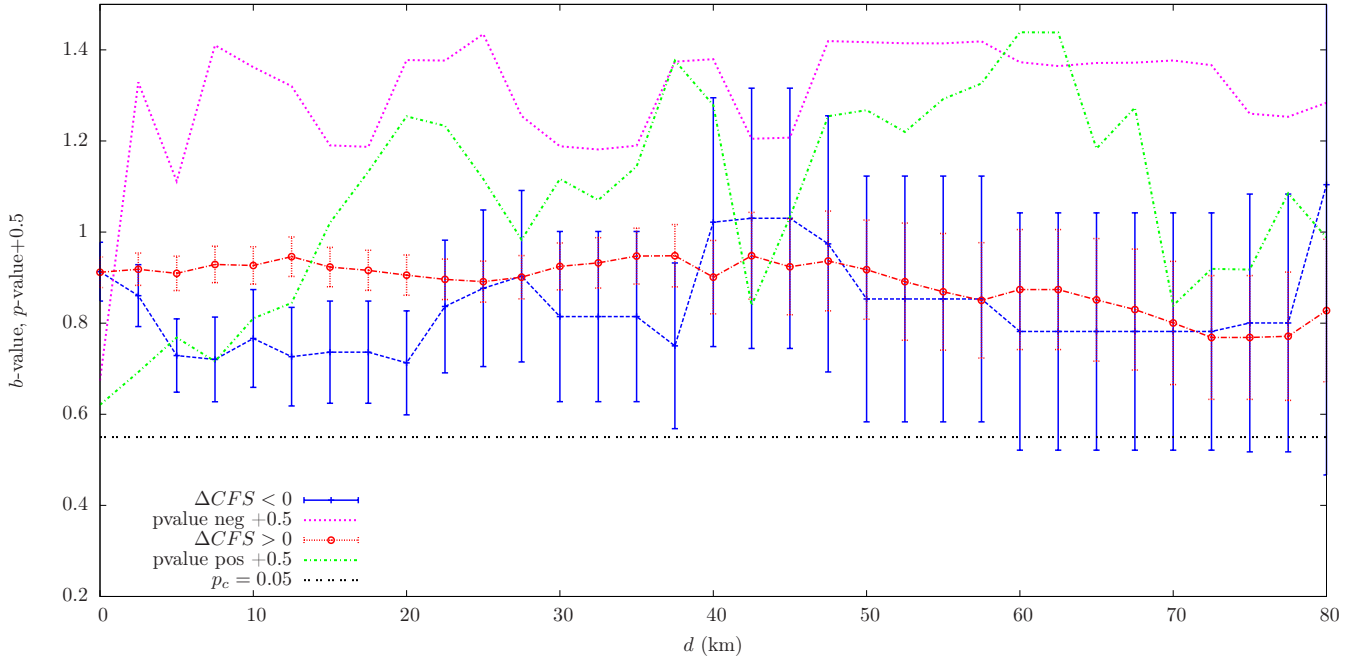


FIG. 6. Dependence of the exponents $b_>$ and $b_<$ (blue and red respectively) on the distance of the events to the fault d for the wald slip model, with $m_{min} = 3$ and $\mu' = 0.4$. Green and purple dashed lines correspond to the p -values of the goodness-of-fit test shifted 0.5 for convenience. Horizontal black dashed line corresponds to the threshold p -value $p_c = 0.05$ shifted 0.5.

	N_{tot}	N	b -value	σ	p_{fit}
Overall	6730	662	$b_{all} = 0.882$	0.034	0.233 ± 0.004
$\mu' = 0.1, \Delta CFS > 0$	5554	564	$b_{>} = 0.906$	0.038	0.385 ± 0.005
$\Delta CFS < 0$	1176	98	$b_{<} = 0.766$	0.077	0.141 ± 0.003
$\mu' = 0.2, \Delta CFS > 0$	5632	573	$b_{>} = 0.900$	0.038	0.255 ± 0.004
$\Delta CFS < 0$	1098	89	$b_{<} = 0.739$	0.078	0.321 ± 0.005
$\mu' = 0.4, \Delta CFS > 0$	5678	580	$b_{>} = 0.909$	0.038	0.267 ± 0.004
$\Delta CFS < 0$	1052	82	$b_{<} = 0.729$	0.081	0.617 ± 0.005
$\mu' = 0.6, \Delta CFS > 0$	5670	582	$b_{>} = 0.909$	0.038	0.264 ± 0.004
$\Delta CFS < 0$	1060	80	$b_{<} = 0.730$	0.082	0.416 ± 0.005
$\mu' = 0.8, \Delta CFS > 0$	5603	583	$b_{>} = 0.906$	0.038	0.263 ± 0.004
$\Delta CFS < 0$	1127	79	$b_{<} = 0.739$	0.083	0.286 ± 0.005

TABLE IV. Results of fitting the Gutenberg-Richter law to the Landers aftershocks, separating positive and negative Coulomb-stress increases as arising from the wald slip model, for different values of the effective friction coefficient μ' and $m_{min} = 3$. The overall case (with ΔCFS taking any sign) is also included and labelled as “all”. Aftershocks correspond to the first 100 days after the Landers mainshock. Distance of aftershocks to the Landers rupture is restricted to be between 5 and 150 km. The p -value of the goodness-of-fit test is computed with 10^4 simulations and is denoted by p_{fit} . Its uncertainty corresponds to one standard deviation. We conclude that the value of μ' has little influence on $b_{>}$ and $b_{<}$.

-
- [1] T. H. Jordan, Y. T. Chen, P. Gasparini, R. Madariaga, I. Main, W. Marzocchi, G. Papadopoulos, G. Sobolev, K. Yamaoka, and J. Zschau. Operational Earthquake Forecasting. State of knowledge and guidelines for utilization. *Annals of Geophysics*, 54, 2011.
- [2] M. Werner, M. Gerstenberger, M. Liukis, W. Marzocchi, D. Rhoades, M. Taroni, J. Zechar, C. Cattania, A. Christophersen, S. Hainzl, A. Helmstetter, A. Jiménez, S. Steacy, and T. Jordan. Retrospective evaluation of time-dependent earthquake forecast models during the 2010-12 Canterbury, New Zealand, earthquake sequence. In *Proceedings of the SSA Annual Meeting, Pasadena (USA)*, 2015.
- [3] A. J. Michael and M. J. Werner. Preface to the focus section on the Collaboratory for the Study of Earthquake Predictability (CSEP): New results and future directions. *Seism. Res. Lett.*, 89(4):1226, 2018.
- [4] C. Cattania, M. J. Werner, W. Marzocchi, S. Hainzl, D. Rhoades, M. Gerstenberger, M. Liukis, W. Savran, A. Christophersen, A. Helmstetter, A. Jiménez, S. Steacy, and T. H. Jordan. The forecasting skill of physics-based seismicity models during the 2010-2012 Canterbury, New Zealand, earthquake sequence. *Seism. Res. Lett.*, 89(4):1238, 2018.
- [5] R.S. Stein, G.C.P. King, and J. Lin. Change in failure stress on the southern San Andreas fault system caused by the 1992 magnitude=7.4 Landers earthquake. *Science*, 258:1328–1332, 1992.
- [6] G. King, R. S. Stein, and J. Lin. Static stress changes and the triggering of earthquakes. *Bull. Seismol. Soc. Am.*, 84:935–953, 1994.
- [7] S. Steacy, J. Gomberg, and M. Cocco. Introduction to special section: stress transfer, earthquake triggering, and time-dependent seismic hazard. *J. Geophys. Res.*, 110:B05S01, 2005.
- [8] S. Nandan, G. Ouillon, J. Woessner, D. Sornette, and S. Wiemer. Systematic assessment of the static stress triggering hypothesis using interearthquake time statistics. *J. Geophys. Res.: Solid Earth*, 121:1890–1909, 2016.
- [9] Takeo Ishibe, Kenji Satake, Shin’ichi Sakai, Kunihiko Shimazaki, Hiroshi Tsuruoka, Yusuke Yokota, Shigeki Nakagawa, and Naoshi Hirata. Correlation between Coulomb stress imparted by the 2011 Tohoku-Oki earthquake and seismicity rate change in Kanto, Japan. *Geophysical Journal International*, 201(1):112–134, 02 2015.

-
- [10] P. Segall, A. L. Llenos, S.-H. Yun, A. M. Bradley, and E. M. Syracuse. Time-dependent dike propagation from joint inversion of seismicity and deformation data. *J. Geophys. Res.: Solid Earth*, 118(11):5785–5804, 2013.
- [11] Simone Cesca, Francesco Grigoli, Sebastian Heimann, Álvaro González, Elisa Buforn, Samira Maghsoudi, Estefania Blanch, and Torsten Dahm. The 2013 September–October seismic sequence offshore Spain: a case of seismicity triggered by gas injection? *Geophysical Journal International*, 198(2):941–953, 06 2014.
- [12] M. Shirzaei, W. L. Ellsworth, K. F. Tiampo, P. J. González, and M. Manga. Surface uplift and time-dependent seismic hazard due to fluid injection in Eastern Texas. *Science*, 353(6306):1416–1419, 2016.
- [13] M. C. Quigley, A. Jiménez, B. Duffy, and T. R. King. Physical and statistical behavior of multifault earthquakes: Darfield earthquake case study, new zealand. *Journal of Geophysical Research: Solid Earth*, 124(5):4788–4810.
- [14] T. Parsons, S. Toda, R. S. Stein, A. Barka, and J. H. Dietrich. Heightened odds of large earthquakes near Istanbul: An interaction-based probability calculation. *Science*, 288:661–665, 2000.
- [15] J. L. Hardebeck, J. J. Nazareth, and E. Hauksson. The static stress change triggering model: Constraints from two southern California aftershock sequences. *J. Geophys. Res.*, 103:24,427–24,437, 1998.
- [16] D. Marsan. Triggering of seismicity at short timescales following Californian earthquakes. *J. Geophys Res.*, 108:1–14, 2003.
- [17] E. P. Mallman and M. D. Zoback. Assessing elastic Coulomb stress transfer models using seismicity rates in southern California and southwestern Japan. *J. Geophys. Res.: Solid Earth*, 112(B3).
- [18] K. R. Felzer and E. E. Brodsky. Testing the stress shadow hypothesis. *J. Geophys. Res.: Solid Earth*, 110(B5).
- [19] B. Gutenberg and C. F. Richter. Frequency of earthquakes in California. *Bull. Seismol. Soc. Am.*, 34:185–188, 1944.
- [20] T. Utsu. Representation and analysis of earthquake size distribution: a historical review and some new approaches. *Pure Appl. Geophys.*, 155:509–535, 1999.
- [21] Y. Y. Kagan. *Earthquakes: Models, Statistics, Testable Forecasts*. Wiley, 2014.

-
- [22] J. Dieterich. A constitutive law for rate of earthquake production and its application to earthquake clustering. *J. Geophys. Res.: Solid Earth*, 99(B2):2601–2618, 1994.
- [23] S. Toda, R.S. Stein, K. Richards-Dinger, and S. Bozkurt. Forecasting the evolution of seismicity in Southern California: Animations built on earthquake stress transfer. *J. Geophys. Res.*, 110:B05S16, 2005.
- [24] C. H. Chan, Y. M. Wu, and J. P. Wang. Earthquake forecasting through a smoothing kernel and the rate-and-state friction law: Application to the Taiwan region. *Nat. Hazards Earth Syst. Sci.*, 12:1–13, 2012.
- [25] C. Cattania, S. Hainzl, L. Wang, F. Roth, and B. Enescu. Propagation of Coulomb stress uncertainties in physics-based aftershock models. *J. Geophys. Res.*, 119:7846–7864, 2014.
- [26] C. Cattania, S. Hainzl, L. Wang, B. Enescu, and F. Roth. Aftershock triggering by postseismic stresses: A study based on Coulomb rate-and-state models. *J. Geophys. Res.*, 120:2388–2407, 2015.
- [27] L. Seeber and J. G. Armbruster. Earthquakes as beacons of stress change. *Nature*, 407:69–72, 2000.
- [28] J. Dieterich, V Cayol, and P. Okubo. The use of earthquake rate changes as a stressmeter at Kilauea volcano. *Nature*, 408:457–460, 2000.
- [29] Y. Kamer and S. Hiemer. Data-driven spatial b value estimation with applications to California seismicity: To b or not to b . *J. Geophys. Res.*, 120(7):5191–5214.
- [30] D. Schorlemmer, S. Wiemer, and M. Wyss. Variations in earthquake-size distribution across different stress regimes. *Nature*, 437:539–542, 2005.
- [31] C. Narteau, S. Byrdina, P. Shebalin, and D. Schorlemmer. Common dependence on stress for the two fundamental laws of statistical seismology. *Nature*, 462:642–645, 2009.
- [32] F. Omori. On the aftershocks of earthquakes. *Journal of the College of Science, Imperial University of Tokyo*, 7:111–200, 1894.
- [33] T. Utsu. A statistical study of the occurrence of aftershocks. *Geophysical Magazine*, 30:521–605, 1961.
- [34] T. Utsu, Y. Ogata, and R.S. Matsu’ura. The centenary of the Omori formula for a decay law of aftershock activity. *J. Phys. Earth*, 43:1–33, 1995.
- [35] Max Wyss and Stefan Wiemer. Change in the probability for earthquakes in southern california due to the landers magnitude 7.3 earthquake. *Science*, 290(5495):1334–1338, 2000.

-
- [36] H. Kanamori and E. E. Brodsky. The physics of earthquakes. *Rep. Prog. Phys.*, 67:1429–1496, 2004.
- [37] D. P. Hill, P. A. Reasenber, A. Michael, W. J. Arabaz, G. Beroza, D. Brumbaugh, J. N. Brune, R. Castro, S. Davis, D. dePolo, W. L. Ellsworth, J. Gomberg, S. Harmsen, L. House, S. M. Jackson, M. J. S. Johnston, L. Jones, R. Keller, S. Malone, L. Munguia, S. Nava, J. C. Pechmann, A. Sanford, R. W. Simpson, R. B. Smith, M. Stark, M. Stickney, A. Vidal, S. Walter, V. Wong, and J. Zollweg. Seismicity remotely triggered by the magnitude 7.3 Landers, California, earthquake. *Science*, 260(5114):1617–1623, 1993.
- [38] E. Hauksson, L. M. Jones, K. Hutton, and D. Eberhart-Phillips. The 1992 Landers earthquake sequence: Seismological observations. *J. Geophys. Res.: Solid Earth*, 98(B11):19835–19858, 1993.
- [39] J. Gomberg, P. A. Reasenber, P. Bodin, and R. A. Harris. Earthquake triggering by seismic waves following the Landers and Hector Mine earthquakes. *Nature*, 411(6836):462–466, May 24 2001.
- [40] D. J. Wald and T. H. Heaton. Spatial and temporal distribution of slip for the 1992 Landers, California, earthquake. *Bull. Seismol. Soc. Am.*, 84(3):668–691, 1994.
- [41] Bruno Hernandez, Fabrice Cotton, and Michel Campillo. Contribution of radar interferometry to a two-step inversion of the kinematic process of the 1992 landers earthquake. *Journal of Geophysical Research: Solid Earth*, 104(B6):13083–13099.
- [42] Sandy Steacy, David Marsan, Suleyman S. Nalbant, and John McCloskey. Sensitivity of static stress calculations to the earthquake slip distribution. *Journal of Geophysical Research: Solid Earth*, 109(B4).
- [43] James A. Spotila and Kerry Sieh. Geologic investigations of a “slip gap” in the surficial ruptures of the 1992 landers earthquake, southern california. *Journal of Geophysical Research: Solid Earth*, 100(B1):543–559.
- [44] E. Hauksson, W. Yang, and P. M. Shearer. Waveform relocated earthquake catalog for Southern California (1981 to june 2011). *Bull. Seismol. Soc. Am.*, 102:2239–2244, October 2012.
- [45] Y. Kamer, G. Ouillon, D. Sornette, and J. Wössner. Condensation of earthquake location distributions: Optimal spatial information encoding and application to multifractal analysis of South Californian seismicity. *Phys. Rev. E*, 92:022808, Aug 2015.

-
- [46] W. Yang, E. Hauksson, and P. M. Shearer. Computing a large refined catalog of focal mechanisms for Southern California (1981-2010): Temporal stability of the style of faulting. *Bull. Seismol. Soc. Am.*, 102:1179–1194, June 2012.
- [47] J. L. Hardebeck and Peter M. Shearer. A new method for determining first-motion focal mechanisms. *Bulletin of the Seismological Society of America*, 92:2264–2276, 2002.
- [48] Y. Okada. Internal deformation due to shear and tensile faults in a half-space. *Bull. Seismol. Soc. Am.*, 82(2):1018–1040, 1992.
- [49] M. Battaglia, P. F. Cervelli, and J. R Murray. dMODELS: A MATLAB software package for modeling crustal deformation near active faults and volcanic centers. *J. Volcanol. Geotherm. Res.*, 254:1 – 4, 2013.
- [50] B. Lautrup. *Physics of Continuous Matter*. CRC Press, 2nd edition, 2011.
- [51] J. McCloskey, S. S. Nalbant, S. Steacy, C. Nostro, O. Scotti, and D. Baumont. Structural constraints on the spatial distribution of aftershocks. *Geophys. Res. Lett.*, 30(12):1610–1613, 2003.
- [52] T. Ishibe, Y. Ogata, H. Tsuruoka, and K. Satake. Testing the Coulomb stress triggering hypothesis for three recent megathrust earthquakes. *Geosci. Lett.*, 4, 2017.
- [53] Paul G Richards Keiiti Aki. *Quantitative seismology*. University Science Books, 2002.
- [54] V. Vavryčuk. Earthquake mechanisms and stress field. In M. Beer, I. A. Kougiumtzoglou, E. Patelli, and I. S.-K. Au, editors, *Encyclopedia of earthquake engineering*. Springer-Verlag, Berlin, 2015.
- [55] M. Cocco and J. R. Rice. Pore pressure and poroelasticity effects in Coulomb stress analysis of earthquake interactions. *J. Geophys. Res.: Solid Earth*, 107(B2):ESE 2–1–ESE 2–17, 2002.
- [56] R. S. Stein. The role of stress transfer in earthquake occurrence. *Nature*, 402:605–609, 1999.
- [57] K. Aki. Maximum likelihood estimate of b in the formula $\log N = a - bm$ and its confidence limits. *Bull. Earthq. Res. Inst. Univ. Tokyo*, 43(2):237–239, 1965.
- [58] W. Marzocchi and L. Sandri. A review and new insights on the estimation of the b -value and its uncertainty. *Annals of Geophysics*, 46(6):1271–1282, 2009.
- [59] B. Bender. Maximum likelihood estimation of b -values for magnitude grouped data. *Bull. Seism. Soc. Am.*, 73:831–851, 1983.
- [60] W. H. Press, S. A. Teukolsky, W. T. Vetterling, and B. P. Flannery. *Numerical Recipes in FORTRAN*. Cambridge University Press, Cambridge, 2nd edition, 1992.

-
- [61] A. Clauset, C. R. Shalizi, and M. E. J. Newman. Power-law distributions in empirical data. *SIAM Rev.*, 51:661–703, 2009.
- [62] A. Deluca and A. Corral. Fitting and goodness-of-fit test of non-truncated and truncated power-law distributions. *Acta Geophys.*, 61:1351–1394, 2013.
- [63] Alvaro Corral and Alvaro Gonzalez. Power law size distributions in geoscience revisited. *Earth and Space Science*, 6(5):673–697.
- [64] J. Woessner and S. Wiemer. Assessing the quality of earthquake catalogues: Estimating the magnitude of completeness and its uncertainty. *Bull. Seismol. Soc. Am.*, 95(2):684–698, 2005.
- [65] Yaolin Shi and Bruce A. Bolt. The standard error of the magnitude-frequency b value. *Bulletin of the Seismological Society of America*, 72(5):1677–1687, 10 1982.
- [66] Y. Pawitan. *In All Likelihood: Statistical Modelling and Inference Using Likelihood*. Oxford UP, Oxford, 2001.
- [67] P. I. Good. *Resampling Methods*. Birkhäuser, Boston, 3rd edition, 2011.
- [68] K. P. Burnham D. R. Anderson. *Model Selection and Multimodel Inference*. Springer-Verlag New York, 2002.
- [69] P. A. Reasenber and L. M. Jones. Earthquake hazard after a mainshock in California. *Science*, 243(4895):1173–1176, 1989.
- [70] L. M. Jones. Foreshocks, aftershocks, and earthquake probabilities: Accounting for the Landers earthquake. *Bull. Seismol. Soc. Am.*, 84(3):892, 1994.
- [71] K. Hutton, J. Woessner, and E. Hauksson. Earthquake monitoring in southern California for seventy-seven years (1932-2008). *Bull. Seismol. Soc. Am.*, 100(2):423, 2010.
- [72] R. Shcherbakov, D. L. Turcotte, and J. B. Rundle. Aftershock statistics. *Pure Appl. Geophys.*, 162(6):1051–1076, 2005.
- [73] V. Navas-Portella, I. Serra, A. Corral, and E. Vives. Increasing power-law range in avalanche amplitude and energy distributions. *Phys. Rev. E*, 97:022134, 2018.
- [74] A. Corral, G. Boleda, and R. Ferrer-i-Cancho. Zipf’s law for word frequencies: Word forms versus lemmas in long texts. *PLoS ONE*, 10(7):e0129031, 2015.
- [75] Paul A. Murtaugh. In defense of p values. *Ecology*, 95(3):611–617.
- [76] David Amitrano. Brittle-ductile transition and associated seismicity: Experimental and numerical studies and relationship with the b value. *Journal of Geophysical Research: Solid Earth*, 108(B1), 2003.

-
- [77] D. E. Smith. *A new paradigm for interpreting stress inversions from focal mechanisms: how 3D stress heterogeneity biases the inversions toward the stress rate*. PhD thesis, California Institute of Technology, 2006.
- [78] Olsen, K. B., Madariaga, R. & Archuleta, R. J. *Three-Dimensional Dynamic Simulation of the 1992 Landers Earthquake*. *Science* **278(5339)**, 834–838 (1997).
- [79] Peyrat, S., Olsen, K. & Madariaga, R. *Dynamic modeling of the 1992 Landers earthquake*. *J. of Geo. Res.: Solid Earth* **106(B11)**, 26467–26482 (2001).
- [80] Mulargia, F. & Bizzarri, A. *Earthquake friction*. *Physics of the Earth and Planetary Interiors* **261**, 118–123 (2016).
- [81] Sabadini, R., Vermeersen, B. & Cambiotti G. *Global Dynamics of the Earth*. 2nd Edition, Springer (2016).

ACKNOWLEDGEMENTS

We are grateful to Álvaro González for some comments on the manuscript, to Paolo Gasperini, Francesco Mulargia, Fabio Romanelli and Roberto Sabadini for the feedback provided during the International Workshop on Seismic Source Physics, Sardinia, and to two anonymous referees who detected some problems in a previous version of the manuscript. The research leading to these results has received founding from “La Caixa” Foundation. V. N. acknowledges financial support from the Spanish Ministry of Economy and Competitiveness (MINECO, Spain), through the “María de Maeztu” Programme for Units of Excellence in R & D (Grant No. MDM-2014-0445). We also acknowledge financial support from MINECO and MICIU under Grants No. FIS2015-71851-P, FIS-PGC2018-099629-B-I00, and “Proyecto Redes de Excelencia” Grant No. MAT2015-69777-REDT. A. J. appreciates the hospitality of the Centre de Recerca Matemàtica.

AUTHOR CONTRIBUTIONS STATEMENT

V. N.-P. and A. J. performed the computations, A. J and A. C. wrote the manuscript. All authors discussed the results and reviewed the manuscript.

COMPETING INTERESTS

The authors declare no competing financial and non-financial interests.